The Journal of Immunology

Rip2 Is Required for Nod2-Mediated Lysozyme Sorting in Paneth Cells

Haifang Wang, Xinwen Zhang, Zhanguang Zuo, Qin Zhang, Ying Pan, Benhua Zeng, Wenxia Li, Hong Wei and Zhihua Liu

J Immunol 2017; 198:3729-3736; Prepublished online 22 March 2017;
doi: 10.4049/jimmunol.1601583
http://www.jimmunol.org/content/198/9/3729

The Journal of Immunology is published twice each month by
The American Association of Immunologists, Inc.,
1451 Rockville Pike, Suite 650, Rockville, MD 20852

Print ISSN: 0022-1767 Online ISSN: 1550-6606.

Rip2 Is Required for Nod2-Mediated Lysozyme Sorting in Paneth Cells

Haifang Wang,*,†,1 Xinwen Zhang,*,†,1 Zhanguang Zuo,*,†,1 Qin Zhang,* Ying Pan,* Benhua Zeng,‡ Wenxia Li,‡ Hong Wei,‡ and Zhihua Liu*,§

Paneth cells play an important role in maintaining intestinal homeostasis by secreting a large number of antimicrobial peptides into the intestinal lumen. In this study, we found that Rip2 is required for lysozyme sorting in Paneth cells in a manner that is dependent on Nod2, LRRK2, and Rab2a. Rip2 deficiency in mouse led to lysosomal degradation of lysozyme in Paneth cells and prevented the recruitment of Rab2a onto dense core vesicles (DCVs). Like Nod2 and LRRK2, Rip2 localizes to DCVs in Paneth cells, and its DCV localization depends on Nod2 and LRRK2. Thus, we delineated a genetic pathway, consisting of Nod2–LRRK2–Rip2–Rab2a, which is required for lysozyme sorting. Taken together, our results indicate that the lysozyme-sorting process in Paneth cells is orchestrated by a number of host factors and highlight the importance of Paneth cell function in intestinal homeostasis. ***The Journal of Immunology*****, 2017, 198: 3729–3736.**

Intestinal homeostasis depends on proper interactions between mucosal immunity and intestinal flora, and intestinal infection or inflammation may occur when the interactions go awry. For example, inflammatory bowel disease, an autoimmune disease with two main forms, Crohn's disease (CD) and ulcerative colitis, is generally thought to develop from an aberrant immune response to intestinal commensal bacteria.

Paneth cells play a vital role in intestinal homeostasis, and their dysfunction may underlie the pathogenesis of inflammatory bowel disease. Paneth cells secrete a large amount of bactericidal factors into the intestinal lumen. The Paneth cell–derived bactericidal factors include lysozyme, Reg3γ, phospholipase PLA2G2A, defensins, and others (1, 2). For convenience, all of the Paneth cell–derived bactericidal factors, including PLA2G2A and lysozyme, despite their large m.w., are hereafter collectively referred to as antimicrobial peptides (AMPs). A number of studies have shown that Paneth cells are critical for the reciprocal relationships between the intestinal epithelium and commensal bacteria by responding to colonization by intestinal bacteria in different ways. For example, Paneth cells upregulate the transcription of a number of AMPs upon colonization by commensal bacteria (3–5). Paneth cells increase AMP secretion upon sensing intestinal bacteria (6). More recently, Paneth cells were found to selectively direct intracellular sorting of lysozyme in response to intestinal bacteria (7).

Abnormalities in Paneth cells are often noted in CD patients (8, 9). Studies in murine models have shown that a number of CD risk factors specifically affect different cellular processes in Paneth cells (10–13), suggesting a causal role for Paneth cell dysfunction in intestinal inflammation. Deletion of the unfolded-protein response transcription factor Xbp1 in mouse intestinal epithelium results in endoplasmic reticulum (ER) stress, a lack of bactericidal factors in Paneth cells, and spontaneous enteritis (10). Atg16L1, an essential gene for autophagy, is required in Paneth cells for proper secretion of lysozyme following norovirus infection in mice (12, 13). Nod2 has been shown to regulate the expression of a subset of defensins in Paneth cells, an effect that might depend on specific genetic background (3, 14–17). Nod2 also participates in the lysozyme-sorting process, and Nod2 deficiency leads to lysosomal degradation of lysozyme in Paneth cells (7). Therefore, abnormalities in pathways within Paneth cells, including AMP production, sorting, and secretion, all likely contribute to the pathogenesis of CD.

Paneth cell–derived AMPs are synthesized in the ER and sorted into specialized secretory dense core vesicles (DCVs) through the Golgi network (18). After budding off the Golgi network, AMP-containing DCVs undergo maturation, during which non–DCV-destined cargos are directed to the endosomal–lysosomal route. Little is known about the mechanisms that determine how DCV cargos, namely AMPs, are retained in DCVs during the maturation process. Our previous study revealed that intestinal bacteria regulate intracellular cargo sorting in Paneth cells (7). The absence of intestinal bacteria in germ-free (GF) mice leads to lysozyme being mistargeted to lysosomes for degradation and a marked reduction

*Key Laboratory of Infection and Immunity, Institute of Biophysics, Chinese Academy of Sciences, Beijing 100101, China; †University of Chinese Academy of Sciences, Beijing 100049, China; ‡Department of Laboratory Animal Science, College of Basic Medical Sciences, Third Military Medical University, Chongqing 400038, China; and §Center for Excellence in Biomacromolecules, Chinese Academy of Sciences, Beijing 100101, China

[1]H. Wang, X.Z., and Z.Z. contributed equally to this work.

ORCIDs: 0000-0002-3536-0618 (Z.Z.); 0000-0002-8043-3900 (B.Z.); 0000-0002-0269-0901 (Z.L.).

Received for publication September 12, 2016. Accepted for publication February 23, 2017.

This work was supported by the National Basic Research Program of China (Grant 2013CB531405), the National Natural Science Foundation of China (Grants 31422019, 31271521, and 31471337), the Thousand Young Talents Program of China, and the Chinese Academy of Sciences (Grant QYZDB-SSW-SMC025).

H. Wang, X.Z., and Z.Z. designed and carried out the majority of the experiments, analyzed results, prepared the figures, and assisted with writing of the manuscript; Q.Z. and Y.P. bred and maintained the different mouse lines and provided guidance on immunostaining and organoid culture; B.Z., W.L., and H. Wei bred and maintained the germ-free mice; and Z.L. designed the project, directed experiments, analyzed data, and wrote the manuscript.

Address correspondence and reprint requests to Dr. Zhihua Liu, Institute of Biophysics, Chinese Academy of Sciences, 15 Datun Road, Room 2707, Chaoyang District, Beijing 100101, China. E-mail address: zhihualiu@ibp.ac.cn

The online version of this article contains supplemental material.

Abbreviations used in this article: AMP, antimicrobial peptide; CD, Crohn's disease; DCV, dense core vesicle; ER, endoplasmic reticulum; Ex-GF, GF mice colonized with conventional microbiota; GF, germ-free; MDP, muramyl dipeptide; PGN, bacterial peptidoglycan; Q-PCR, quantitative PCR; RT, room temperature; SPF, specific pathogen–free; TAB, TAK1 binding protein; TAK1, TGF-β–activating kinase 1; WT, wild-type.

in lysozyme in the intestinal lumen. Correct sorting of lysozyme during DCV maturation in conventionally raised mice requires Nod2. Mechanistically, upon sensing its cognate ligand, Nod2 recruits LRRK2 and Rab2a onto the DCV surface to direct lysozyme sorting during DCV maturation. This bacterium-directed sorting is a lysozyme-specific phenomenon, because sorting of other AMPs is not altered in GF mice or *Nod2*$^{-/-}$mice.

Nod2 and its homolog Nod1 are the founding members of the Nod-like receptor family, which detect intracellular bacteria by sensing bacterial peptidoglycan (PGN). Nod1 is more widely expressed, whereas Nod2 expression is limited to certain cell types, including Paneth cells and hematopoietic cells (19, 20). Nod1 and Nod2 share a common pathway in initiating a proinflammatory response that is dependent on activation of NF-κB and MAPKs by recruiting the adaptor protein Rip2 (21). Nod proteins undergo oligomerization upon binding PGN fragments, which results in recruitment and activation of Rip2 (21–23). Rip2-deficient macrophages do not respond to Nod1 or Nod2 ligands (24, 25). Activation of Rip2 recruits and activates the TGF-β–activating kinase 1 (TAK1)–TAK1-binding protein (TAB)2–TAB3 complex, which subsequently activates the canonical NF-κB pathway and MAPK signaling pathway to induce inflammatory responses (26).

It is unknown whether Nod2-directed lysozyme sorting requires other essential components in the known Nod2–Rip2–TAK1–NF-κB signaling pathway. Notably, Rip2 also locates to a CD-susceptibility locus (27). In this study, we sought to determine whether Rip2 is implicated in the Nod2-mediated lysozyme-sorting process.

Materials and Methods

Mice

Rip2$^{-/-}$, *Lrrk2*$^{-/-}$, and *Nod2*$^{-/-}$ mice on a C57BL/6J background were described previously (7, 23). All specific pathogen–free (SPF) mice, including wild-type (WT) C57BL/6J mice, were bred and housed in an American Association for the Accreditation of Laboratory Animal Care–accredited barrier facility for SPF mice at Tsinghua University. The facility is routinely monitored for the absence of specific infectious agents, including murine norovirus and *Helicobacter*. GF C57BL/6J mice were maintained in GF conditions in vinyl isolators in the animal facility. Mice were euthanized immediately upon being taken out of isolators. Animals were used according to protocols approved by the Institutional Animal Care and Use Committee.

GF C57BL/6J mice were bred and maintained in GF conditions in vinyl isolators in the animal facility at Third Military Medical University and used according to protocols approved by the Institutional Animal Care and Use Committee. The GF status was routinely confirmed by in-house aerobic and anaerobic cultures of feces. Mice were euthanized immediately upon being taken out of isolators. Bacterial colonization of GF mice was performed by inoculating GF mice with feces from SPF mice for 2 wk before analysis.

Abs

The following primary Abs were used: anti-LRRK2 (Epitomics; MJFF2 c41-2), anti-lysozyme (Abcam; ab36362), anti-Rab2a (sc-28567), anti-Rab10 (sc-6564), Nod2 Ab (H-300) (all from Santa Cruz Biotechnology; sc-30199), Rip2 Abs for immunostaining (Abcam; ab8428) and for immunoblotting (Abnova; H0000876-M02), and anti-actin (Sigma; AC15). The PerCP-Cy5.5–conjugated anti-CD24 Ab was from eBioscience. A rabbit anti-procryptdin Ab was developed in-house, as described previously (7). Fluorophore-conjugated secondary Abs were from Invitrogen.

Reagents

All chemical reagents were from Sigma, unless otherwise specified. The TAK1 inhibitor 5Z-7-oxozeaenol was from Calbiochem (499610). GSK583 and WEHI-345 were purchased from MedchemExpress.

Isolation of CD24^{+} Paneth cells

Crypts from small intestine were isolated as described (7). Briefly, mice were euthanized, and a 5-cm section of distal ileum was harvested. The distal ileum with fat and connective tissues removed was flushed with cold PBS and opened longitudinally. Then the tissue was washed vigorously in cold PBS, chopped into <3–4 mm^2 pieces, and incubated with 2 ml of 0.1% collagenase solution at 37°C for 30 min. The digestion reaction was mixed by pipetting up and down every 5 min. The digestion was repeated for another 30 min in 2 ml of fresh 0.1% collagenase solution. When ∼70% of the crypts were released, 10 ml of cold PBS was added to stop the digestion. The released crypts were filtered through a 70-μm cell strainer and pelleted by centrifugation at 100 × *g* for 5 min. A further digestion with TrypLE Express, supplemented with 2000 U/ml DNase I, was performed to isolate single cells. The resulting single cells were stained with a PerCP-Cy5.5–conjugated anti-CD24 Ab in PBS supplemented with 2% FBS. Labeled single cells were sorted into two populations, CD24^{-} and CD24^{+}, which were collected and subjected to immunoblotting analysis.

Gastrointestinal Listeria monocytogenes *infection*

Gastrointestinal *L. monocytogenes* infection was performed as described (7). Briefly, sex- and age-matched (6–8-wk-old) WT and *Rip2*$^{-/-}$ littermates were used for the infection experiments, which were performed under BL2 conditions. Mice were infected via gastric gavage with 10^9 *L. monocytogenes* strain 10403s per mouse. Bacterial burden, measured in CFU, was assayed. Feces were collected under sterile conditions 10 h postinfection, and bacterial burden was presented as CFU/mg dry weight.

Recombinant lysozyme supplementation

Sex- and age-matched (6–8-wk-old) WT and *Rip2*$^{-/-}$ littermates were fed 100 mg/kg recombinant lysozyme (Sigma) or PBS by gastric gavage every 24 h for seven consecutive days. Twenty-four hours after the final treatment, mice were infected with 10^9 *L. monocytogenes* by gastric gavage. Bacterial burden was measured as described above.

Fluorescent immunohistochemical staining of tissue sections

Staining of tissue sections was performed as described (7). Briefly, tissue slices (6 μm thick) from paraffin-embedded murine ileum of different genotypes were mounted on positively charged glass and dewaxed. Slides were blocked with PBS supplemented with 10% normal goat serum after Ag retrieval in 0.01 M sodium citrate buffer (pH 6) for 25 min in a boiling steamer. Tissue slides were then labeled with primary Abs at 4°C overnight and with fluorophore-conjugated secondary Abs at room temperature (RT) for 2 h. Goat serum (10%) was present throughout all Ab incubation steps. Slides were washed with PBS three times for 5 min between each incubation step, counterstained with TO-PRO-3, and mounted in Fluoromount-G (Southern Biotech). Confocal images were obtained with a Zeiss LSM 700 imaging system under 63× oil objectives.

In vivo muramyl dipeptide treatment of GF mice

GF mice in vinyl isolators were administered muramyl dipeptide (MDP) orally (500 μg per mouse) in 100 μl of endotoxin-free PBS, or PBS (sham) twice, 12 h apart. Four hours after the second treatment, mice were sacrificed, and intestinal tissues were harvested.

Intestinal organoid culture and treatment

Intestinal organoids were cultured as previously described (7). Briefly, crypts were isolated from small intestine as described above. Pelleted crypts (∼500) were suspended in 50 μl of Matrigel (Invitrogen) and plated in a 24-well plate, supplemented with 500 μl of growth medium per well. Growth medium was changed every 3 or 4 d. Every week, organoids were retrieved from the Matrigel, dissociated mechanically, mixed with fresh Matrigel, and plated into a 24-well plate. Organoid growth medium contained Advanced DMEM/F12 with L-glutamine, 1% Pen/Strep, 10 μM HEPES (all from Invitrogen), N2 supplement 1:100 (R&D Systems), B27 supplement 1:50 (Invitrogen), 10 ng/ml Wnt-3a, 50 ng/ml EGF, 100 ng/ml Noggin, and 500 ng/ml R-spondin (all from PeproTech).

Cultured organoids were treated with leupeptin (100 μM), gefitinib (2.5 μM), GSK583 (5 μM), WEHI-345 (2.5 μM), or 5Z-7-oxozeaenol (20 nM) or were mock treated for 16 h in growth medium before being washed, fixed, and processed for immunostaining, or alternatively, harvested for immunoblotting.

Image-based quantification of positively stained DCVs

Quantification was performed by a blinded investigator. DCVs in 30 Paneth cells from each individual animal were quantified. Results from the specified number of animals were averaged and plotted using GraphPad Prism software.

Immunofluorescence staining of cultured organoids

For staining, organoids were grown on glass coverslips. After the indicated treatment, organoids were washed with ice-cold PBS once and fixed with ice-cold 4% paraformaldehyde in PBS for 15 min. After PBS washes, organoids were blocked with Ab dilution buffer (PBS supplemented with 10% goat serum and 0.1% saponin) for 30 min and incubated with primary Abs at 4˚C overnight, followed by fluorophore-conjugated secondary Abs at RT for 2 h. Washing with PBS containing 0.1% Tween-20 was performed three times for each step. After coverslips were mounted onto slides in Fluoromount-G and air dried, confocal images were obtained with a Zeiss LSM 700 imaging system under a 63× oil objective.

Whole-mount immunofluorescence staining

After mice were euthanized, ileal sections were harvested, opened longitudinally with the adipose tissues stripped off, and fixed with 4% paraformaldehyde in PBS for 1 h. After PBS washes, ileal tissues were labeled with an anti-lysozyme Ab in PBS supplemented with 10% normal goat serum for 2 h at RT. After PBS washes, tissues were incubated with FITC-conjugated *Helix pomatia* lectin (Invitrogen; L11271) and PE-conjugated anti-mouse IgG1 secondary Ab for 2 h at RT. Tissues were mounted on glass slides and examined under a Nikon Eclipse 90i automated fluorescence microscope with a 10× objective.

Isolation and quantification of mRNA

RNA was extracted with TRIzol Reagent (Invitrogen), following the manufacturer's instructions. cDNA was transcribed using a PrimerScript RT Reagent Kit (Takara). Quantitative PCR (Q-PCR) reactions were performed in triplicate using Light Cycler SYBR Green DNA Master Mix (Takara) on an ABI 7500 thermal cycler. The following thermal cycling conditions were used: 50˚C for 2 min, 95˚C for 10 min, 40 cycles of 95˚C for 15 s, and 60˚C for 1 min. The specificity of Q-PCR was verified with melting curves of each PCR reaction. The level of target mRNA was determined by the difference of cycle threshold values between the target and loading control. The level of mouse GAPDH mRNA was used as the control to normalize loading. The following primers were used for Q-PCR: mouse Rip2-Forward: 5′-ATCCCGTACCACAAGCTCG-3′; mouse Rip2-Reverse: 5′-GGATGTGTAGGTGCTTCACTG-3′; mouse lysozyme1-Forward: 5′-GCCAAGGTCTACAATCGTTGTGAGTTG-3′; mouse lysozyme1-Reverse: 5′-GCCAAGGTCTACAATCGTTGTGAGTTG-3′; mouse GAPDH-Forward: 5′-GGTCCTCAGTGTAGCCCAAG-3′; and mouse GAPDH-Reverse: 5′-AATGTGTCCGTCGTGGATCT-3′.

Statistical analysis

The statistical tests used are stated in the individual figure legends. GraphPad Prism software was used for calculations. The results are expressed as the mean ± SEM, unless otherwise indicated.

Results

Paneth cells express a high level of Rip2

To determine whether Rip2 was involved in Nod2-mediated lysozyme sorting in Paneth cells, we first examined whether Rip2 was expressed in Paneth cells. We isolated Paneth cells from WT murine ileum using the surface marker CD24 (28). Rip2 mRNA was highly enriched in $CD24^+$ Paneth cells (Fig. 1A). Immunoblotting analysis also detected Rip2 in purified $CD24^+$ Paneth cells (Fig. 1B). The immunoblotting was validated by detection of Rip2 in bone marrow cells from WT and $Rip2^{-/-}$ mice (Fig. 1B). Notably, the expression of Rip2 was not exclusive to Paneth cells; it was also detected in $CD24^-$ cells. Thus, Paneth cells, as well as regular epithelial cells, express Rip2.

Localization of Nod2 to the DCV surface in Paneth cells is required for lysozyme sorting; thus, we examined the cellular distribution of Rip2 in Paneth cells. DCVs were labeled with an Ab that detects their authentic cargo, procryptdin. Immunofluorescence staining of Rip2 in ileal sections from WT mice revealed that it was highly concentrated on the procryptdin$^+$ DCV surface (Fig. 1C). To validate our immunostaining results, we performed immunostaining on ileal sections from $Rip2^{-/-}$ mice in parallel and found that there was no notable Rip2 signal. Therefore, Rip2 localizes on the DCV surface in Paneth cells.

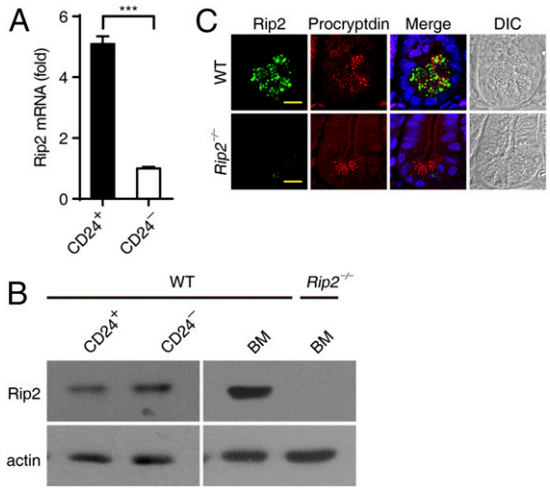

FIGURE 1. Rip2 is expressed in Paneth cells. (**A**) Relative mRNA level of Rip2 in sorted $CD24^+$ and $CD24^-$ cells from isolated murine crypt cells determined by Q-PCR. The mRNA level of GAPDH was used for normalization. (**B**) Immunoblotting analysis of Rip2 in cell lysates prepared from sorted cells in (A) or bone marrow (BM) in WT or $Rip2^{-/-}$ mice. Actin was used as a loading control. (**C**) Fluorescent immunohistochemical confocal images of Rip2 (green) in crypt sections from WT or $Rip2^{-/-}$ mice. Procryptdin (red) was used as a marker for Paneth cells. Staining in WT or $Rip2^{-/-}$ tissues was performed simultaneously. Nuclei were counterstained with Hoechst 33342 (blue). Differential interference contrast (DIC) images are also shown (right panels). Scale bars, 10 μm. Data are taken from three independent experiments (A) or are representative of three independent experiments (B and C). $***p < 0.001$, Student *t* test.

The presence of microbiota promotes DCV localization of Rip2

The localization of Nod2 on DCVs depends on the presence of intestinal microbiota. To determine whether commensal bacteria also regulate DCV recruitment of Rip2, we compared the cellular distribution of Rip2 in conventionally raised SPF mice, GF mice, and GF mice colonized with conventional microbiota (Ex-GF). Because the Abs against Rip2 and procryptdin were rabbit derived, we chose a DCV-localized GTPase, Rab10, as the marker for DCVs in Paneth cells. Rab10 colocalized well with procryptdin in Paneth cells, and its DCV localization did not depend on the presence of microbiota, Nod2, or LRRK2 (7). Compared with SPF mice, the DCV localization of Rip2 in GF mice was greatly reduced (Fig. 2A, 2B). Colonization with intestinal flora restored the DCV localization of Rip2, as shown in Ex-GF samples (Fig. 2A, 2B). Furthermore, treatment of GF mice with the Nod2 cognate ligand MDP restored the localization of Rip2 on the DCV surface, suggesting that Nod2 signaling was involved (Fig. 2C). Therefore, DCV localization of Rip2 also depends on Nod2 binding its ligand.

Rip2 deficiency renders Paneth cells devoid of lysozyme in mature DCVs

DCVs undergo a maturation process after budding off the *trans*-Golgi network, during which DCV cargos are condensed, and non–DCV-destined cargos are redirected to the endosome/lysosome route. DCVs travel toward the plasma membrane during maturation. Thus, in polarized cells, such as Paneth cells, the relative cellular localization of DCVs reveals their maturation status: more mature DCVs, which are ready for release, are located on the apical side, whereas the relatively nascent and immature DCVs, referred to in this article as subapical, are located away from the apical side. The sorting of lysozyme during DCV maturation depends on sensing of PGN by Nod2. In $Nod2^{-/-}$

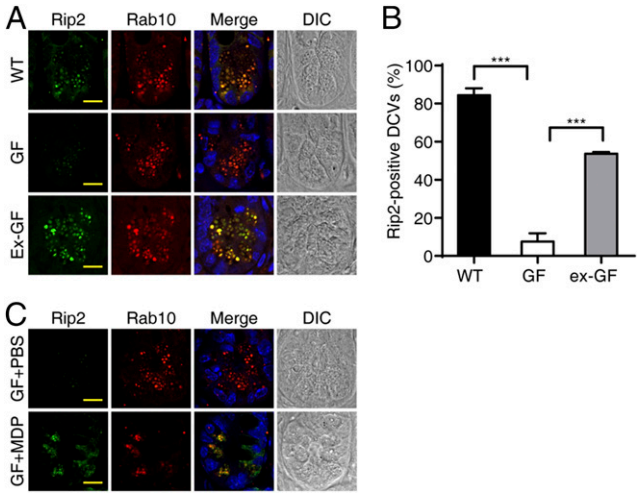

FIGURE 2. Localization of Rip2 to DCVs is microbiota dependent. (**A**) Confocal images of Rip2 and Rab10 in ileal sections from SPF, GF, and Ex-GF mice. Blue, counterstained nuclei. Scale bar, 10 μm. (**B**) Percentage of $Rip2^+$ DCVs in (A). DCVs from 30 Paneth cells per mouse were quantified in three animals for each condition. Data are expressed as mean ± SEM. (**C**) Confocal images of Rip2 and Rab10 in ileal sections from GF mice treated with PBS or MDP. Data are representative of three independent experiments (A and C). $***p < 0.001$, Student *t* test.

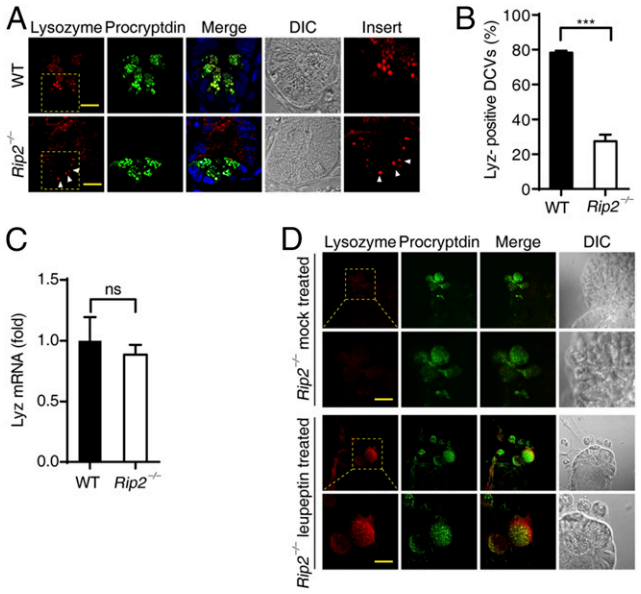

FIGURE 3. Rip2 deficiency reduces the amount of lysozyme in Paneth cells. (**A**) Immunohistochemical confocal images of lysozyme (red) and procryptidin (green) in crypt sections from WT or $Rip2^{-/-}$ mice. Blue, counterstained nuclei. Boxed areas are enlarged (2×) in the far right panels (Insert). White arrowheads indicate lysozyme-positive subapical DCVs. Scale bars, 10 μm. (**B**) Percentage of lysozyme-positive (lyz-positive) DCVs in WT and $Rip2^{-/-}$ Paneth cells from (A). DCVs from 30 Paneth cells per mouse were quantified in three animals for each genotype. Data are expressed as mean ± SEM. (**C**) Relative mRNA level of lysozyme in sorted $CD24^+$ cells from isolated WT or $Rip2^{-/-}$ crypts. The mRNA level of GAPDH was used for normalization. $p > 0.05$, Student *t* test. (**D**) Confocal images of lysozyme and procryptidin in cultured $Rip2^{-/-}$ crypt organoids treated with leupeptin (100 μM) or mock treated for 24 h. Boxed areas are showed at higher magnification in the panels underneath. Scale bars, 10 μm. Data are taken from three independent experiments (C) or are representative of three independent experiments (A and D). $***p < 0.001$, Student *t* test. ns, nonsignificant.

Paneth cells, lysozyme is mistargeted to lysosomes for degradation so that lysozyme is present in a few subapical immature DCVs but not in apical mature DCVs (7). To determine whether Rip2 is also involved in the lysozyme-sorting process, we performed immunostaining of lysozyme in ileal crypts from WT and $Rip2^{-/-}$ mice. In WT crypts, lysozyme and procryptidin colocalized well in DCVs (Fig. 3A), which was confirmed by quantification (Fig. 3B). However, in $Rip2^{-/-}$ crypts, lysozyme staining was observed mostly in the subapical immature DCVs (Fig. 3A, 3B). The phenomenon that lysozyme staining in $Rip2^{-/-}$ crypts was restricted to subapical immature DCVs (Fig. 3A, dashed boxes) suggests that there is probably a gradual loss of lysozyme during DCV maturation, similar to the defect observed in $Nod2^{-/-}$ Paneth cells. Therefore, we used Q-PCR analysis to quantify lysozyme mRNA in WT and $Rip2^{-/-}$ crypts. Q-PCR analysis showed comparable levels of lysozyme in crypts isolated from WT and $Rip2^{-/-}$ mice (Fig. 3C). Thus, the reduced amount of lysozyme in $Rip2^{-/-}$ Paneth cells was likely due to a defect in a posttranslational process, such as an altered cargo-sorting process. To examine whether lysozyme was degraded in lysosomes in $Rip2^{-/-}$ Paneth cells, we cultured small intestinal organoids. These organoids contained authentic Paneth cells that could be visualized by procryptidin staining (28). Consistent with our in vivo observation, lysozyme was readily detectable in WT Paneth cells but markedly reduced in $Rip2^{-/-}$ Paneth cells (Supplemental Fig. 1). Furthermore, we treated $Rip2^{-/-}$ organoids with leupeptin, a lysosome inhibitor. Compared with DMSO treatment, leupeptin treatment restored lysozyme staining in cultured $Rip2^{-/-}$ Paneth cells (Fig. 3D). Staining of whole mounts of ileum showed colocalization of lysozyme with mucus (detected by lectin–*Helix pomatia* agglutinin staining) in the intestinal lumen of WT mice; however, lysozyme staining was significantly reduced in the intestinal lumen of $Rip2^{-/-}$ mice (Supplemental Fig. 2A). In comparison, procryptidin staining in the intestinal lumen was similar in WT and $Rip2^{-/-}$ mice (Supplemental Fig. 2B), indicating normal DCV exocytosis. Thus, similar to defects observed in $Nod2^{-/-}$ or $Lrrk2^{-/-}$ Paneth cells (7), Rip2 deficiency leads to a specific impairment in the sorting process for lysozyme but not other cargos, such as procryptidin, in Paneth cells.

To examine whether reduced lysozyme in $Rip2^{-/-}$ Paneth cells impairs bacterial clearance in the gastrointestinal tract, we orally challenged WT and $Rip2^{-/-}$ mice with *L. monocytogenes*. We found that Rip2 deficiency led to more *L. monocytogenes* present in feces (Supplemental Fig. 2C), indicating less bactericidal activity. Furthermore, supplementation with recombinant lysozyme restored bacterial clearance in $Rip2^{-/-}$ mice (Supplemental Fig. 2C), indicating that the reduced level of lysozyme in $Rip2^{-/-}$ mice contributed to reduced bacterial control.

Small GTPases are the master regulators of intracellular membrane trafficking. Rab2a is a small GTPase that has been implicated in directing ER–Golgi trafficking and cargo sorting during DCV maturation (29). Although Rab2a and Rab10 localize to DCVs in Paneth cells, Rab2a is required for lysozyme sorting during DCV maturation (7). Because Rab2a is the key small GTPase required for lysozyme sorting, we sought to determine whether Rip2 participated in lysozyme sorting through a Rab2a-dependent pathway. We first examined the DCV localization of Rab2a in WT and $Rip2^{-/-}$ Paneth cells. Because the Abs against Rab2a and procryptidin were rabbit derived, and the Ab against Rab10 was mouse derived, we used Rab10 in place of procryptidin to mark DCVs in Paneth cells. Rab2a staining was ubiquitous on $Rab10^+$ DCVs in WT cells (Fig. 4A), whereas, in $Rip2^{-/-}$ Paneth cells, Rab2a staining was absent from apical mature DCVs but

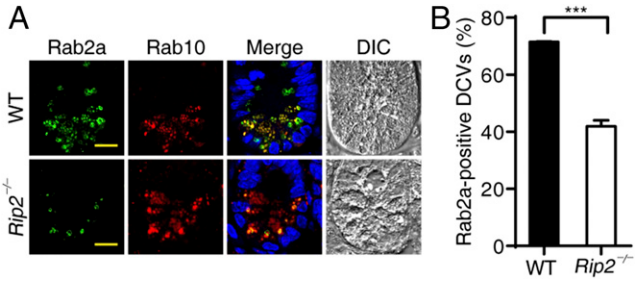

FIGURE 4. Rip2 is required for DCV localization of Rab2a in Paneth cells. (**A**) Confocal images of Rab2a and Rab10 in WT and *Rip2*$^{-/-}$ ileal sections. Blue, counterstained nuclei. Scale bars, 10 μm. Data are representative of at least five independent experiments. (**B**) Percentage of Rab2a^{+} DCVs in (A). DCVs from 30 Paneth cells per mouse were quantified in each genotype. Data are expressed as mean ± SEM. ***$p < 0.001$, Student *t* test.

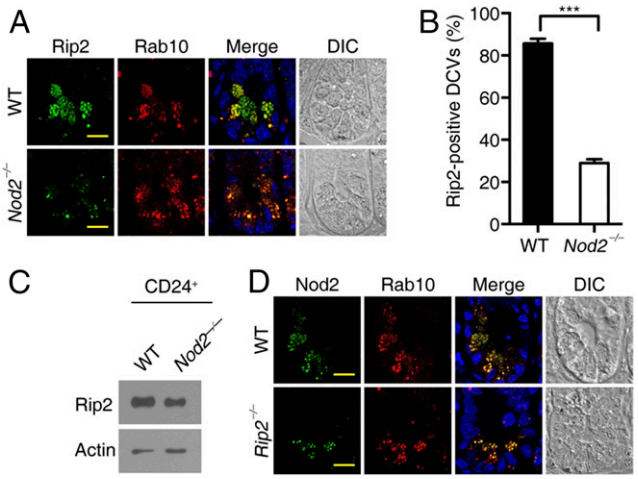

FIGURE 5. Nod2 is required for DCV localization of Rip2 in Paneth cells. (**A**) Confocal images of Rip2 and Rab10 in WT and *Nod2*$^{-/-}$ ileal sections. Blue, counterstained nuclei. Scale bars, 10 μm. (**B**) Percentage of Rip2a^{+} DCVs in (A). DCVs from 30 Paneth cells per mouse were quantified in each genotype. Data are expressed as mean ± SEM. (**C**) Immunoblotting analysis of Rip2 in sorted CD24^{+} Paneth cells from WT and *Nod2*$^{-/-}$ intestinal crypts. Actin was used as a loading control. (**D**) Confocal images of Nod2 and Rab10 in WT and *Rip2*$^{-/-}$ ileal sections. Blue, counterstained nuclei. Scale bars, 10 μm. Data are representative of at least five independent experiments (A and D) and two independent experiments (C). ***$p < 0.001$, Student *t* test.

was present on the subapical immature DCVs (Fig. 4A). The data on DCV localization of Rab2a in WT and *Rip2*$^{-/-}$ Paneth cells are quantified in Fig. 4B, which shows a significant reduction in Rab2a DCV localization in *Rip2*$^{-/-}$ Paneth cells. Thus, Rip2 is required for lysozyme sorting, likely through regulating DCV targeting of Rab2a.

Rip2 acts downstream of Nod2 and LRRK2 in directing lysozyme sorting

PGN fragments from intestinal microbiota promote DCV localization of Nod2, LRRK2, and Rab2a to direct lysozyme sorting in Paneth cells. We focus hereafter on DCV recruitment of Nod2, LRRK2, and Rip2 to delineate how Rip2 participates in the lysozyme-sorting pathway. To determine whether Rip2 acts downstream of Nod2, we examined the cellular localization of Rip2 in WT and *Nod2*$^{-/-}$ Paneth cells. Compared with WT Paneth cells, the DCV localization of Rip2 in *Nod2*$^{-/-}$ Paneth cells was markedly reduced (Fig. 5A, 5B), suggesting that Nod2 is required for DCV recruitment of Rip2. Of note, the reduced staining of Rip2 in *Nod2*$^{-/-}$ Paneth cells was not due to a reduced amount of Rip2. Our immunoblotting indicated comparable levels of Rip2 in sorted WT and *Nod2*$^{-/-}$ Paneth cells (Fig. 5C). Under our experimental conditions, diffuse cytosolic staining is less visible than punctate staining on DCVs. DCV localization of Nod2 in WT and *Rip2*$^{-/-}$ Paneth cells was comparable (Fig. 5D), suggesting that it occurs independently of Rip2.

We next sought to determine the DCV localization of LRRK2 and Rip2 in *Rip2*$^{-/-}$ and *Lrrk2*$^{-/-}$ Paneth cells, respectively. The DCV localization of LRRK2 was comparable in WT and *Rip2*$^{-/-}$ Paneth cells (Fig. 6A, 6B), suggesting that DCV localization of LRRK2 does not require Rip2. However, the DCV localization of Rip2 was markedly reduced in *Lrrk2*$^{-/-}$ Paneth cells compared with WT Paneth cells (Fig. 6C, 6D), suggesting that DCV localization of Rip2 depends on LRRK2. Thus, these results place Rip2 downstream of LRRK2. Together, our results indicate that a genetic pathway consisting of Nod2–LRRK2–Rip2–Rab2a is required for lysozyme sorting in Paneth cells.

Rip2 kinase activity is not required for lysozyme sorting

To determine whether the kinase activity of Rip2 is required for the Nod2-dependent lysozyme-sorting process, we treated organoids with gefitinib, an inhibitor of the EGFR tyrosine kinase that also inhibits Rip2 kinase activity (30). Treatment of WT Paneth cells with gefitinib did not alter the staining of lysozyme, even at the highest concentration (2.5 μM) that we used without visible toxicity to cultured organoids (Fig. 7A). Similarly, treatment of WT Paneth cells with GSK583 or WEHI-345, both of which are specific inhibitors of Rip2 kinase activity, did not alter the staining of lysozyme (Supplemental Fig. 3A, 3B). The data suggest that Rip2 kinase activity is not required for lysozyme sorting.

TAK1 is a key kinase downstream of Rip2 in Nod2-mediated NF-κB activation. We sought to determine whether TAK1 is involved in lysozyme sorting. We first determined the TAK1 expression pattern in Paneth cells. TAK1 was detected in isolated crypt cells (Supplemental Fig. 3C). Immunohistochemical staining showed that TAK1 localized to the DCV surface, but its localization was not changed in *Nod2*$^{-/-}$ and *Rip2*$^{-/-}$ Paneth cells (Supplemental Fig. 3D, 3E). This probably indicates that TAK1 is not involved in Nod2-mediated lysozyme sorting. To further determine whether the kinase activity of TAK1 was involved, we treated cultured organoids with 5Z-7-oxozeaenol, a TAK1 inhibitor. Treatment with this TAK1 inhibitor did not affect lysozyme staining in Paneth cells (Fig. 7B). Thus, taken together, our results suggest that Rip2 kinase activity and TAK1 are not involved in lysozyme sorting.

Discussion

In this study, we uncovered a role for Rip2 in lysozyme sorting in Paneth cells using our genetic approach. By immunostaining, we found that Rip2 is highly expressed in Paneth cells and localizes to the DCV surface. Rip2 deficiency caused a marked reduction in lysozyme in apical mature DCVs, suggesting a sorting defect during DCV maturation. Consistent with this, lysosome inhibition restored lysozyme in cultured *Rip2*$^{-/-}$ Paneth cells, and Rip2 deficiency reduced the DCV localization of Rab2a on apical mature DCVs. These results demonstrated that Rip2 is indeed involved in lysozyme sorting in Paneth cells, most likely in a Rab2a-dependent manner. Nod2 and LRRK2 are required for DCV localization of Rip2 but not vice versa. Using chemical inhibitors, we showed that the kinase activity of Rip2 or TAK1 is not required for lysozyme sorting. Thus, our study finds that lysozyme sorting is regulated by a genetic pathway consisting of Nod2–LRRK2–Rip2–Rab2a in Paneth cells.

In myeloid cells, cytosolic PGN fragments induce autophagy and activate inflammatory signaling (21, 22). In contrast, as this study and

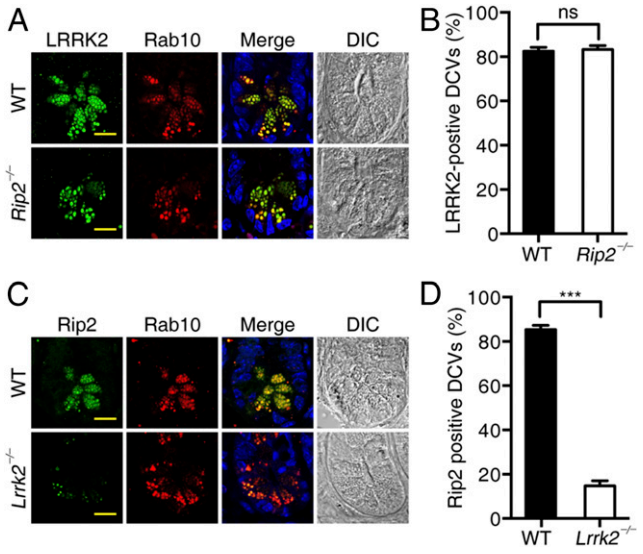

FIGURE 6. LRRK2 is required for localization of Rip2 to DCVs in Paneth cells. (**A**) Confocal images of Rip2 and Rab10 in WT and *Lrrk2*$^{-/-}$ ileal sections. Blue, counterstained nuclei. Scale bars, 10 μm. (**B**) Percentage of Rip2a^{+} DCVs in (A). DCVs from 30 Paneth cells per mouse were quantified in each genotype. Data are expressed as mean ± SEM. (**C**) Confocal images of LRRK2 and Rab10 in WT and *Rip2*$^{-/-}$ ileal sections. Blue, counterstained nuclei. Scale bars, 10 μm. (**D**) Percentage of LRRK2^{+} DCVs in (C). DCVs from 30 Paneth cells per mouse were quantified in each genotype. Data are expressed as mean ± SEM. Data are representative of at least five independent experiments (A and C). ***$p < 0.001$, Student t test. ns, nonsignificant ($p < 0.05$).

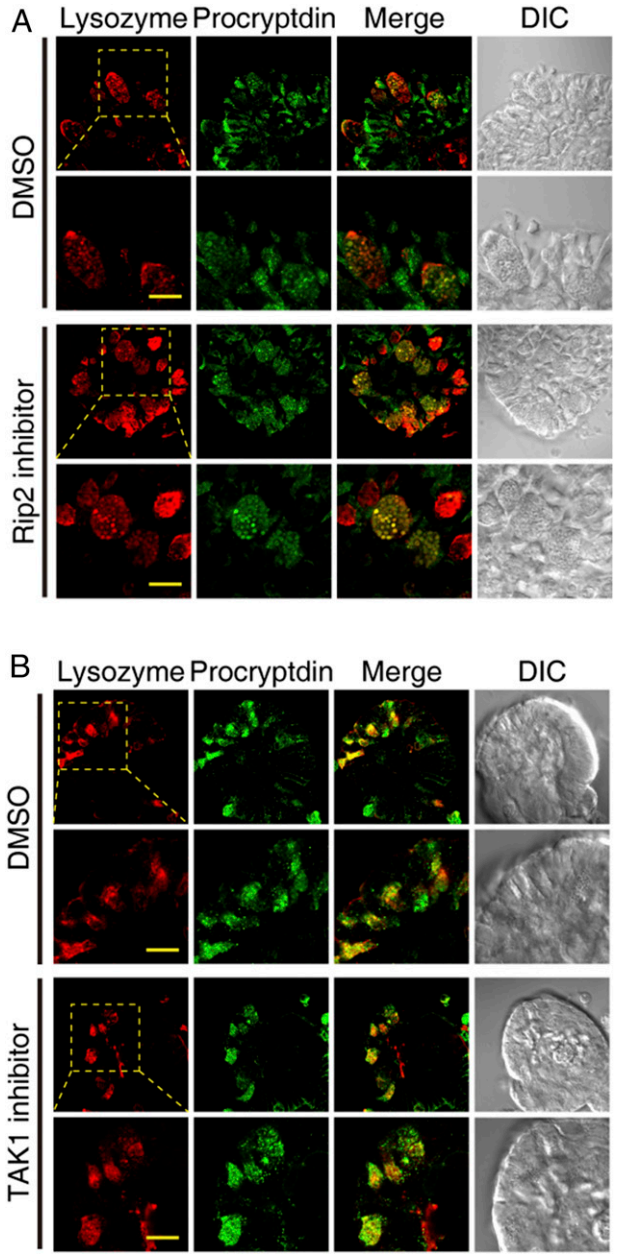

FIGURE 7. The kinase activity of Rip2 is not required for lysozyme sorting in Paneth cells. Confocal images of lysozyme and procryptdin in cultured WT crypt organoids treated with gefitinib (2.5 μM) or mock treated (**A**) or treated with 5Z-7-oxozeaenol (20 nM) or mock treated (**B**) for 24 h. Boxed areas are shown at higher magnification in the panels underneath. Scale bars, 10 μm. Data are representative of at least three independent experiments.

our previous studies show, cytosolic PGN fragments in Paneth cells initiate lysozyme sorting through a Nod2–LRRK2–Rip2–Rab2a pathway. The gut lumen contains abundant free PGN (31), which may be generated from cleavage of PGN chains by lytic transglycosylases during bacterial cell division. The free PGN may be taken up by Paneth cells through endocytosis, endosomal membrane transporters, transmembrane channels, or bacterial outer membrane vesicles (32–34). Therefore, cytosolic PGN in Paneth cells most likely represents microbial signals derived from commensal bacteria and initiates a noninflammatory process of lysozyme sorting. In comparison, intracellular PGN in myeloid cells is more likely to occur as a result of a bacterial infection, which calls for autophagic induction and proinflammatory responses to initiate innate and adaptive immune reactions to eliminate infection. Thus, one pathogen-associated molecular pathway elicits distinct pathways, exemplifying the complexity and versatility of host–microbe interactions.

Although Rip2 is indispensable for NF-κB activation, its role in other Nod2-driven processes can be more complicated and sometimes warrants further investigation. For example, Nod2 induces microRNA-29 expression in human dendritic cells to limit IL-23 release (35), but it remains to be determined whether this process is Rip2 dependent. Nod2 deficiency leads to abnormalities in intestinal goblet cells and overgrowth of the commensal *Bacteroides vulgatus* in a Rip2-dependent manner (36). The requirement for Rip2 in Nod1- and Nod2-mediated autophagy depends on the nature of the cell type and stimuli. Autophagy induced by the Gram-negative bacterium *Shigella flexneri* is Rip2 independent, because bacterium-induced autophagy remains intact in Rip2-deficient mouse embryo fibroblasts (37). In comparison, MDP-induced autophagy depends on Nod2 and Rip2 in the human intestinal epithelial cell line HCT116 or dendritic cells (38, 39). Similarly, PGN-containing outer membrane vesicles induce autophagy in a manner that is dependent on Nod1 and Rip2 (40). A recent study showed that ER stress induces inflammation in a Nod1/Nod2- and Rip2-dependent manner (41). Our study demonstrates a requirement for Rip2 in Nod2-mediated lysozyme sorting in Paneth cells, but in a kinase activity–independent manner, which adds another dimension of complexity to the mechanism by which Rip2 acts as a key mediator downstream of Nod2.

The presence of intestinal microbiota is required for the sorting of lysozyme in Paneth cells (7). Our data show that MDP enhances the recruitment of Rip2 to the DCV surface in Paneth cells. We suspect that the effect from microbes can be both direct and indirect. On the one hand, MDP from microbes may directly promote DCV localization of Nod2, which subsequently recruits Rip2. On the other hand, signals from microbes may further modulate the expression levels of Nod2, Rip2, and other related

proteins in Paneth cells. Thus, the overall effect of enhanced localization of Rip2 on DCVs in the presence of microbes may reflect the complex nature of microbes on host regulation. Nevertheless, Nod2, LRRK2, or Rip2 deficiency results in defective sorting of lysozyme. Furthermore, Nod2 and LRRK2 are required for DCV localization of Rip2, whereas DCV localization of Nod2 or LRRK2 does not require Rip2, indicating that Nod2 and LRRK2 are upstream of Rip2. Because Nod2 is required for LRRK2 localization to DCVs, we propose that a genetic pathway consisting of Nod2–LRRK2–Rip2–Rab2a is responsible for lysozyme sorting in Paneth cells. It is surprising that LRRK2 is required for Rip2 localization to DCVs, because it is generally believed that the interaction between Nod2 and Rip2 should be sufficient to bring Rip2 to the membrane (33). A likely scenario is that LRRK2 is needed to enhance or stabilize the Nod2–Rip2 complex triggered by commensal bacterium–derived signaling in Paneth cells. Indeed, modifiers of the Nod2–Rip2 complex have been identified. For example, conjugation of lys63-linked or linear-linked polyubiquitin chains to Rip2 by a number of E3 ligases plays a critical role in Nod2-induced NF-κB activation (26, 39, 42–44). It is of interest to determine whether LRRK2 indeed modulates the Nod2–Rip2 complex in Paneth cells. A surprising finding is that the kinase activity of Rip2 is not required for the DCV recruitment of Rab2a. Therefore, a likely scenario is that Rip2 directly or indirectly recruits Rab2a onto the DCV surface. Characterizing protein interactions biochemically in Paneth cells is technically challenging because, despite much effort, there is no immortalized Paneth cell line, and primary Paneth cells do not grown in a pure population (45, 46). Furthermore, DCVs are highly specialized organelles that are only present in neurons and endocrine cells, ruling out the possibility of studying the lysozyme-sorting process in regular cell lines. Therefore, genetic identification may offer a practical alternative for the identification of important players required in the lysozyme-sorting pathway in Paneth cells.

Nod2 and LRRK2 are encoded by CD-susceptibility genes (16, 17, 47, 48). Our study reveals that Rip2 participates in lysozyme sorting through a Nod2–LRRK2–Rip2–Rab2a pathway in Paneth cells in response to intestinal commensal bacteria. Our discovery once again highlights the importance of proper host–microbe interactions in maintaining intestinal homeostasis.

Acknowledgments

We thank Dr. Yihui Xu for assistance with imaging, Dr. Xiaoyan Wang for assistance with FACS sorting, and Xudong Zhao and Xiaofei Guo for technical assistance with equipment. We thank Dr. Hongliang Li, Wuhan University, for sharing mouse strains with us.

Disclosures

The authors have no financial conflicts of interest.

References

1. Bevins, C. L., and N. H. Salzman. 2011. Paneth cells, antimicrobial peptides and maintenance of intestinal homeostasis. *Nat. Rev. Microbiol.* 9: 356–368.
2. Clevers, H. C., and C. L. Bevins. 2013. Paneth cells: maestros of the small intestinal crypts. *Annu. Rev. Physiol.* 75: 289–311.
3. Vaishnava, S., C. L. Behrendt, A. S. Ismail, L. Eckmann, and L. V. Hooper. 2008. Paneth cells directly sense gut commensals and maintain homeostasis at the intestinal host-microbial interface. *Proc. Natl. Acad. Sci. USA* 105: 20858–20863.
4. Cash, H. L., C. V. Whitham, C. L. Behrendt, and L. V. Hooper. 2006. Symbiotic bacteria direct expression of an intestinal bactericidal lectin. *Science* 313: 1126–1130.
5. El Aidy, S., P. van Baarlen, M. Derrien, D. J. Lindenbergh-Kortleve, G. Hooiveld, F. Levenez, J. Doré, J. Dekker, J. N. Samsom, E. E. Nieuwenhuis, and M. Kleerebezem. 2012. Temporal and spatial interplay of microbiota and intestinal mucosa drive establishment of immune homeostasis in conventionalized mice. *Mucosal Immunol.* 5: 567–579.
6. Ayabe, T., D. P. Satchell, C. L. Wilson, W. C. Parks, M. E. Selsted, and A. J. Ouellette. 2000. Secretion of microbicidal alpha-defensins by intestinal Paneth cells in response to bacteria. *Nat. Immunol.* 1: 113–118.
7. Zhang, Q., Y. Pan, R. Yan, B. Zeng, H. Wang, X. Zhang, W. Li, H. Wei, and Z. Liu. 2015. Commensal bacteria direct selective cargo sorting to promote symbiosis. *Nat. Immunol.* 16: 918–926.
8. Dvorak, A. M., and G. R. Dickersin. 1980. Crohn's disease: transmission electron microscopic studies. I. Barrier function. Possible changes related to alterations of cell coat, mucous coat, epithelial cells, and Paneth cells. *Hum. Pathol.* 11(Suppl. 5): 561–571.
9. VanDussen, K. L., T. C. Liu, D. Li, F. Towfic, N. Modiano, R. Winter, T. Haritunians, K. D. Taylor, D. Dhall, S. R. Targan, et al. 2014. Genetic variants synthesize to produce Paneth cell phenotypes that define subtypes of Crohn's disease. *Gastroenterology* 146: 200–209.
10. Kaser, A., A. H. Lee, A. Franke, J. N. Glickman, S. Zeissig, H. Tilg, E. E. Nieuwenhuis, D. E. Higgins, S. Schreiber, L. H. Glimcher, and R. S. Blumberg. 2008. XBP1 links ER stress to intestinal inflammation and confers genetic risk for human inflammatory bowel disease. *Cell* 134: 743–756.
11. Adolph, T. E., M. F. Tomczak, L. Niederreiter, H. J. Ko, J. Böck, E. Martinez-Naves, J. N. Glickman, M. Tschurtschenthaler, J. Hartwig, S. Hosomi, et al. 2013. Paneth cells as a site of origin for intestinal inflammation. *Nature* 503: 272–276.
12. Cadwell, K., J. Y. Liu, S. L. Brown, H. Miyoshi, J. Loh, J. K. Lennerz, C. Kishi, W. Kc, J. A. Carrero, S. Hunt, et al. 2008. A key role for autophagy and the autophagy gene Atg16l1 in mouse and human intestinal Paneth cells. *Nature* 456: 259–263.
13. Cadwell, K., K. K. Patel, N. S. Maloney, T. C. Liu, A. C. Ng, C. E. Storer, R. D. Head, R. Xavier, T. S. Stappenbeck, and H. W. Virgin. 2010. Virus-plus-susceptibility gene interaction determines Crohn's disease gene Atg16L1 phenotypes in intestine. *Cell* 141: 1135–1145.
14. Kobayashi, K. S., M. Chamaillard, Y. Ogura, O. Henegariu, N. Inohara, G. Nuñez, and R. A. Flavell. 2005. Nod2-dependent regulation of innate and adaptive immunity in the intestinal tract. *Science* 307: 731–734.
15. Shanahan, M. T., I. M. Carroll, E. Grossniklaus, A. White, R. J. von Furstenberg, R. Barner, A. A. Fodor, S. J. Henning, R. B. Sartor, and A. S. Gulati. 2014. Mouse Paneth cell antimicrobial function is independent of Nod2. *Gut* 63: 903–910.
16. Hugot, J. P., M. Chamaillard, H. Zouali, S. Lesage, J. P. Cézard, J. Belaiche, S. Almer, C. Tysk, C. A. O'Morain, M. Gassull, et al. 2001. Association of NOD2 leucine-rich repeat variants with susceptibility to Crohn's disease. *Nature* 411: 599–603.
17. Ogura, Y., D. K. Bonen, N. Inohara, D. L. Nicolae, F. F. Chen, R. Ramos, H. Britton, T. Moran, R. Karaliuskas, R. H. Duerr, et al. 2001. A frameshift mutation in NOD2 associated with susceptibility to Crohn's disease. *Nature* 411: 603–606.
18. Kim, T., M. C. Gondré-Lewis, I. Arnaoutova, and Y. P. Loh. 2006. Dense-core secretory granule biogenesis. *Physiology (Bethesda)* 21: 124–133.
19. Inohara, N., T. Koseki, L. del Peso, Y. Hu, C. Yee, S. Chen, R. Carrio, J. Merino, D. Liu, J. Ni, and G. Núñez. 1999. Nod1, an Apaf-1-like activator of caspase-9 and nuclear factor-kappaB. *J. Biol. Chem.* 274: 14560–14567.
20. Ogura, Y., S. Lala, W. Xin, E. Smith, T. A. Dowds, F. F. Chen, E. Zimmermann, M. Tretiakova, J. H. Cho, J. Hart, et al. 2003. Expression of NOD2 in Paneth cells: a possible link to Crohn's ileitis. *Gut* 52: 1591–1597.
21. Philpott, D. J., M. T. Sorbara, S. J. Robertson, K. Croitoru, and S. E. Girardin. 2014. NOD proteins: regulators of inflammation in health and disease. *Nat. Rev. Immunol.* 14: 9–23.
22. Caruso, R., N. Warner, N. Inohara, and G. Núñez. 2014. NOD1 and NOD2: signaling, host defense, and inflammatory disease. *Immunity* 41: 898–908.
23. Kobayashi, K., N. Inohara, L. D. Hernandez, J. E. Galán, G. Núñez, C. A. Janeway, R. Medzhitov, and R. A. Flavell. 2002. RICK/Rip2/CARDIAK mediates signalling for receptors of the innate and adaptive immune systems. *Nature* 416: 194–199.
24. Park, J. H., Y. G. Kim, C. McDonald, T. D. Kanneganti, M. Hasegawa, M. Body-Malapel, N. Inohara, and G. Núñez. 2007. RICK/RIP2 mediates innate immune responses induced through Nod1 and Nod2 but not TLRs. *J. Immunol.* 178: 2380–2386.
25. Magalhaes, J. G., J. Lee, K. Geddes, S. Rubino, D. J. Philpott, and S. E. Girardin. 2011. Essential role of Rip2 in the modulation of innate and adaptive immunity triggered by Nod1 and Nod2 ligands. *Eur. J. Immunol.* 41: 1445–1455.
26. Yang, Y., C. Yin, A. Pandey, D. Abbott, C. Sassetti, and M. A. Kelliher. 2007. NOD2 pathway activation by MDP or *Mycobacterium tuberculosis* infection involves the stable polyubiquitination of Rip2. *J. Biol. Chem.* 282: 36223–36229.
27. Jostins, L., S. Ripke, R. K. Weersma, R. H. Duerr, D. P. McGovern, K. Y. Hui, J. C. Lee, L. P. Schumm, Y. Sharma, C. A. Anderson, et al; International IBD Genetics Consortium (IIBDGC). 2012. Host-microbe interactions have shaped the genetic architecture of inflammatory bowel disease. *Nature* 491: 119–124.
28. Sato, T., J. H. van Es, H. J. Snippert, D. E. Stange, R. G. Vries, M. van den Born, N. Barker, N. F. Shroyer, M. van de Wetering, and H. Clevers. 2011. Paneth cells constitute the niche for Lgr5 stem cells in intestinal crypts. *Nature* 469: 415–418.
29. Sumakovic, M., J. Hegermann, L. Luo, S. J. Husson, K. Schwarze, C. Olendrowitz, L. Schoofs, J. Richmond, and S. Eimer. 2009. UNC-108/RAB-2 and its effector RIC-19 are involved in dense core vesicle maturation in *Caenorhabditis elegans*. *J. Cell Biol.* 186: 897–914.
30. Tigno-Aranjuez, J. T., J. M. Asara, and D. W. Abbott. 2010. Inhibition of RIP2's tyrosine kinase activity limits NOD2-driven cytokine responses. *Genes Dev.* 24: 2666–2677.
31. Clarke, T. B., K. M. Davis, E. S. Lysenko, A. Y. Zhou, Y. Yu, and J. N. Weiser. 2010. Recognition of peptidoglycan from the microbiota by Nod1 enhances systemic innate immunity. *Nat. Med.* 16: 228–231.

32. Kaparakis-Liaskos, M., and R. L. Ferrero. 2015. Immune modulation by bacterial outer membrane vesicles. *Nat. Rev. Immunol.* 15: 375–387.
33. Nakamura, N., J. R. Lill, Q. Phung, Z. Jiang, C. Bakalarski, A. de Mazière, J. Klumperman, M. Schlatter, L. Delamarre, and I. Mellman. 2014. Endosomes are specialized platforms for bacterial sensing and NOD2 signalling. *Nature* 509: 240–244.
34. Dalmasso, G., H. T. Nguyen, S. A. Ingersoll, S. Ayyadurai, H. Laroui, M. A. Charania, Y. Yan, S. V. Sitaraman, and D. Merlin. 2011. The PepT1-NOD2 signaling pathway aggravates induced colitis in mice. *Gastroenterology* 141: 1334–1345.
35. Brain, O., B. M. Owens, T. Pichulik, P. Allan, E. Khatamzas, A. Leslie, T. Steevels, S. Sharma, A. Mayer, A. M. Catuneanu, et al. 2013. The intracellular sensor NOD2 induces microRNA-29 expression in human dendritic cells to limit IL-23 release. *Immunity* 39: 521–536.
36. Ramanan, D., M. S. Tang, R. Bowcutt, P. Loke, and K. Cadwell. 2014. Bacterial sensor Nod2 prevents inflammation of the small intestine by restricting the expansion of the commensal *Bacteroides vulgatus*. *Immunity* 41: 311–324.
37. Travassos, L. H., L. A. Carneiro, M. Ramjeet, S. Hussey, Y. G. Kim, J. G. Magalhães, L. Yuan, F. Soares, E. Chea, L. Le Bourhis, et al. 2010. Nod1 and Nod2 direct autophagy by recruiting ATG16L1 to the plasma membrane at the site of bacterial entry. *Nat. Immunol.* 11: 55–62.
38. Homer, C. R., A. Kabi, N. Marina-García, A. Sreekumar, A. I. Nesvizhskii, K. P. Nickerson, A. M. Chinnaiyan, G. Nuñez, and C. McDonald. 2012. A dual role for receptor-interacting protein kinase 2 (RIP2) kinase activity in nucleotide-binding oligomerization domain 2 (NOD2)-dependent autophagy. *J. Biol. Chem.* 287: 25565–25576.
39. Cooney, R., J. Baker, O. Brain, B. Danis, T. Pichulik, P. Allan, D. J. Ferguson, B. J. Campbell, D. Jewell, and A. Simmons. 2010. NOD2 stimulation induces autophagy in dendritic cells influencing bacterial handling and antigen presentation. *Nat. Med.* 16: 90–97.
40. Irving, A. T., H. Mimuro, T. A. Kufer, C. Lo, R. Wheeler, L. J. Turner, B. J. Thomas, C. Malosse, M. P. Gantier, L. N. Casillas, et al. 2014. The immune receptor NOD1 and kinase RIP2 interact with bacterial peptidoglycan on early endosomes to promote autophagy and inflammatory signaling. *Cell Host Microbe* 15: 623–635.
41. Keestra-Gounder, A. M., M. X. Byndloss, N. Seyffert, B. M. Young, A. Chávez-Arroyo, A. Y. Tsai, S. A. Cevallos, M. G. Winter, O. H. Pham, C. R. Tiffany, et al. 2016. NOD1 and NOD2 signalling links ER stress with inflammation. *Nature* 532: 394–397.
42. Damgaard, R. B., U. Nachbur, M. Yabal, W. W. Wong, B. K. Fiil, M. Kastirr, E. Rieser, J. A. Rickard, A. Bankovacki, C. Peschel, et al. 2012. The ubiquitin ligase XIAP recruits LUBAC for NOD2 signaling in inflammation and innate immunity. *Mol. Cell* 46: 746–758.
43. Hasegawa, M., Y. Fujimoto, P. C. Lucas, H. Nakano, K. Fukase, G. Núñez, and N. Inohara. 2008. A critical role of RICK/RIP2 polyubiquitination in Nod-induced NF-kappaB activation. *EMBO J.* 27: 373–383.
44. Bertrand, M. J., K. Doiron, K. Labbé, R. G. Korneluk, P. A. Barker, and M. Saleh. 2009. Cellular inhibitors of apoptosis cIAP1 and cIAP2 are required for innate immunity signaling by the pattern recognition receptors NOD1 and NOD2. *Immunity* 30: 789–801.
45. Garabedian, E. M., L. J. Roberts, M. S. McNevin, and J. I. Gordon. 1997. Examining the role of Paneth cells in the small intestine by lineage ablation in transgenic mice. *J. Biol. Chem.* 272: 23729–23740.
46. Sato, T., R. G. Vries, H. J. Snippert, M. van de Wetering, N. Barker, D. E. Stange, J. H. van Es, A. Abo, P. Kujala, P. J. Peters, and H. Clevers. 2009. Single Lgr5 stem cells build crypt-villus structures in vitro without a mesenchymal niche. *Nature* 459: 262–265.
47. Franke, A., D. P. McGovern, J. C. Barrett, K. Wang, G. L. Radford-Smith, T. Ahmad, C. W. Lees, T. Balschun, J. Lee, R. Roberts, et al. 2010. Genome-wide meta-analysis increases to 71 the number of confirmed Crohn's disease susceptibility loci. *Nat. Genet.* 42: 1118–1125.
48. Anderson, C. A., G. Boucher, C. W. Lees, A. Franke, M. D'Amato, K. D. Taylor, J. C. Lee, P. Goyette, M. Imielinski, A. Latiano, et al. 2011. Meta-analysis identifies 29 additional ulcerative colitis risk loci, increasing the number of confirmed associations to 47. *Nat. Genet.* 43: 246–252.

Supplementary Figures

Supplementary Figure 1

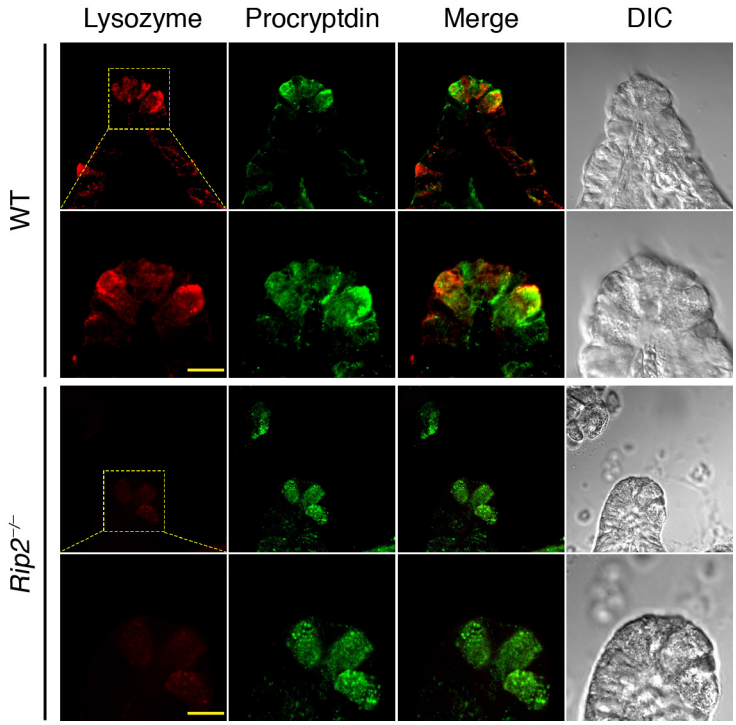

Supplementary Figure 1. Rip2 deficiency leads to decreased amounts of lysozyme in cultured Paneth cells. Confocal images of lysozyme and procryptdin in cultured WT and *Rip2*$^{-/-}$ crypt organoids. Boxed areas are further magnified in the lower panels. Scale bars, 10 μm. Data are representative of three independent experiments.

Supplementary Figure 2

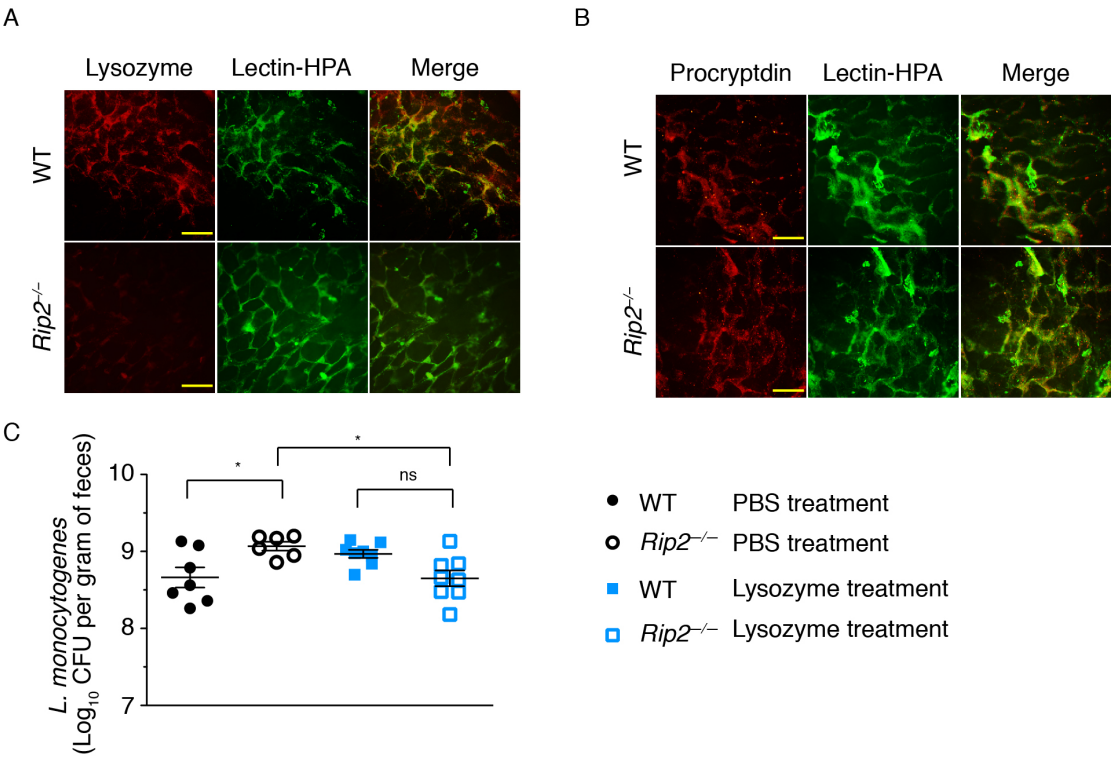

Supplementary Figure 2. Rip2 deficiency leads to decreased amounts of lysozyme in the intestinal lumen. Whole-mount images from WT and *Rip2*$^{-/-}$ mice taken immediately above the ileal mucosal surface and stained with *Helix pomatia* lectin (lectin-HPA) and antibodies against lysozyme (**A**) or procryptdin (**B**). Scale bars, 100 μm. (**C**) Numbers of bacteria (colony-forming units (CFU)) present in feces 10 h after infection with 10^9 CFU of *L. monocytogenes* by oral gavage in WT and *Rip2*$^{-/-}$ mice. * $P < 0.05$; ns, $P > 0.05$ (two-way ANOVA with Tukey's test). Each symbol represents an individual animal; horizontal bars indicate median values with sem. Data are representative of three independent experiments (A, B) and two independent experiments (**C**).

Supplementary Figure 3

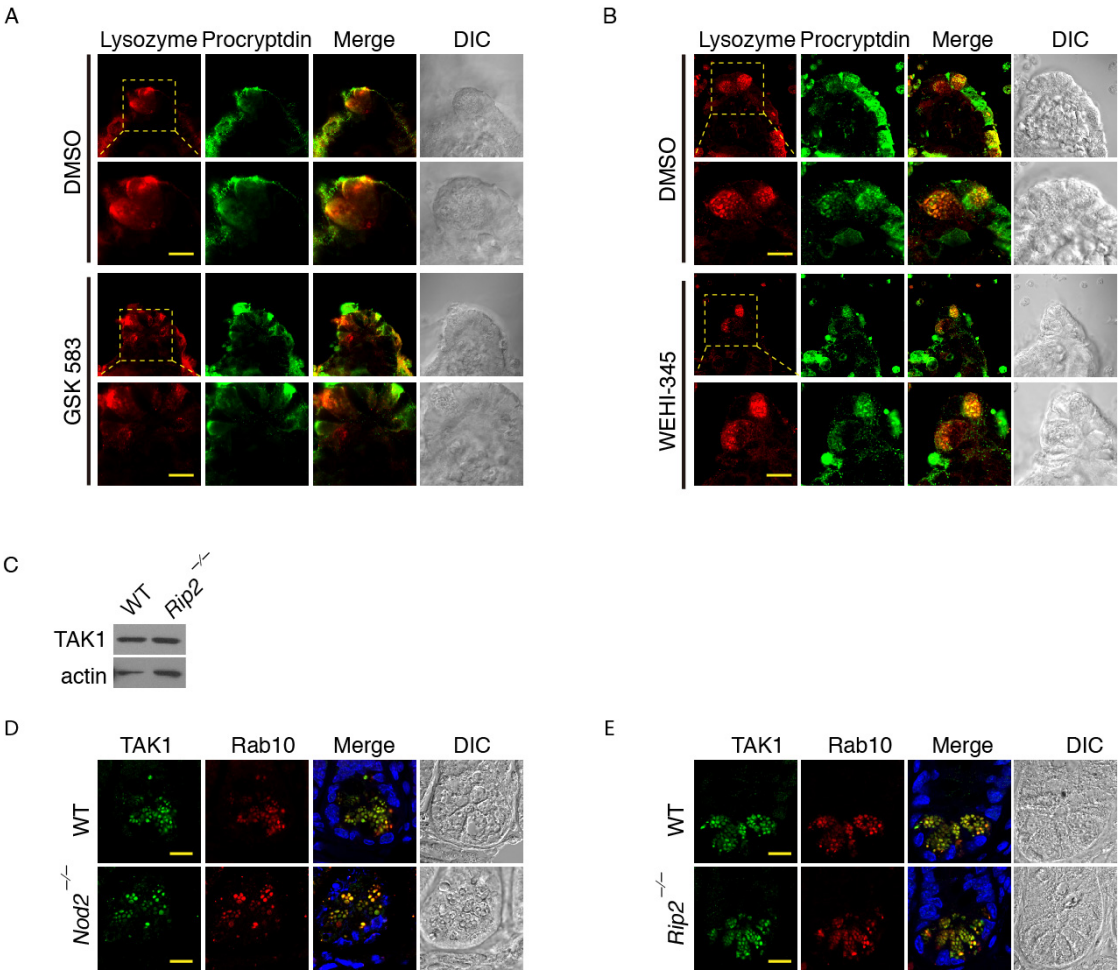

Supplementary Figure 3. The kinase activity of Rip2 and TAK1 are not required for lysozyme sorting. (**A-B**) Confocal images of lysozyme and procryptdin in cultured WT crypt organoids treated with GSK583 (5 μM) or mock-treated (**A**), or WEHI-345 (2.5 μM) or mock-treated (**B**) for 16 hours. Boxed areas are further magnified in the lower panels. Scale bars, 10 μm. (**C**) Immunoblotting analysis of TAK1 in isolated crypt cells from WT and *Rip2*$^{-/-}$ mice. Actin was used as a loading control. (**D**, **E**) Confocal images of TAK1 and Rab10 in murine ileal sections from WT and *Nod2*$^{-/-}$ (**D**) or *Rip2*$^{-/-}$ (**E**) mice. Blue, counterstained nuclei. Scale bars, 10 μm. Data are representative of three independent experiments.